Septal cholinergic neurons gate hippocampal output to entorhinal cortex via oriens lacunosum moleculare interneurons

Juhee Haam[a], Jingheng Zhou[a], Guohong Cui[a], and Jerrel L. Yakel[a,1]

[a]Neurobiology Laboratory, National Institute of Environmental Health Sciences, National Institutes of Health, Department of Health and Human Services, Research Triangle Park, NC 27709

Edited by Bruce S. McEwen, The Rockefeller University, New York, NY, and approved January 12, 2018 (received for review July 13, 2017)

Neuromodulation of neural networks, whereby a selected circuit is regulated by a particular modulator, plays a critical role in learning and memory. Among neuromodulators, acetylcholine (ACh) plays a critical role in hippocampus-dependent memory and has been shown to modulate neuronal circuits in the hippocampus. However, it has remained unknown how ACh modulates hippocampal output. Here, using in vitro and in vivo approaches, we show that ACh, by activating oriens lacunosum moleculare (OLM) interneurons and therefore augmenting the negative-feedback regulation to the CA1 pyramidal neurons, suppresses the circuit from the hippocampal area CA1 to the deep-layer entorhinal cortex (EC). We also demonstrate, using mouse behavior studies, that the ablation of OLM interneurons specifically impairs hippocampus-dependent but not hippocampus-independent learning. These data suggest that ACh plays an important role in regulating hippocampal output to the EC by activating OLM interneurons, which is critical for the formation of hippocampus-dependent memory.

acetylcholine | oriens lacunosum moleculare interneurons | hippocampus | memory | photometry

Memory formation consists of two distinct phases, memory encoding and consolidation. Memory encoding refers to the initial memory-formation process where sensory inputs from the neocortex are transferred to the hippocampus (1, 2). During memory consolidation, on the other hand, the encoded temporary hippocampal information is transferred back to the neocortex for long-term storage of the memory. Previous studies have indicated that memory encoding and consolidation interfere with each other and are temporally separated (3–7). As such, memory encoding is dominant when an animal is actively learning, whereas consolidation occurs during sleep when sensory inputs are minimal (3, 5, 7). However, the mechanism behind this regulation remains elusive.

Acetylcholine (ACh) plays a crucial role in memory function, the significance of which is well known in patients with Alzheimer's disease who manifest a substantial loss of cholinergic neurons (8, 9). ACh plays a unique role in learning and memory by differentially modulating memory encoding and consolidation. The levels of ACh in the hippocampus are high during active memory encoding but low during slow-wave sleep, when memory consolidation is dominant (6, 10, 11). Furthermore, pharmacological studies showed that ACh not only stimulates memory encoding but also inhibits consolidation while encoding actively occurs (4, 6, 12–14). In vitro examination of synaptic plasticity using slice electrophysiology and optical imaging have shown that ACh stimulates the Schaffer collateral pathway in the hippocampus to increase memory encoding (15–18). It remains unclear, however, whether ACh modulates the circuits involved in memory consolidation, especially the hippocampus to the entorhinal cortex (EC) circuit, which is the gateway to the consolidation pathway.

The EC plays a critical role in memory formation via acting as an interface between the cortex and the hippocampus. Principal cells in the EC, which are glutamatergic neurons, provide extrinsic connections with other cortical and subcortical regions. The principal neurons in the superficial EC layers (layers II and III) receive sensory inputs from the neocortex and project to the hippocampus for memory encoding during active learning (19–21). The superficial EC layers project to hippocampal area CA1 via the trisynaptic pathway (EC–dentate gyrus–CA3–CA1) as a part of the encoding pathway or directly to the CA1 via the temporoammonic pathway (EC–CA1), which has been shown to be critical for memory consolidation (22). On the other hand, principal neurons in deep EC layers (mainly layer V) receive direct hippocampal output and convey the information back to the cortex for memory consolidation (23, 24). Additionally, the deep-layer EC neurons also project to the superficial layer of the EC to complete the loop of the hippocampus–entorhinal cortical circuit (25, 26), acting as a hub in the hippocampus–EC circuit.

The negative-feedback mechanism is an effective way to tightly control the output of information. Oriens lacunosum moleculare (OLM) cells in the hippocampal area CA1 are major negative-feedback regulators of the hippocampal output neurons (i.e., CA1 pyramidal neurons). OLM neurons receive excitatory inputs from the CA1 pyramidal neurons while providing inhibitory inputs to these CA1 pyramidal neurons. Each OLM interneuron forms more than 10,000 synaptic boutons in the stratum lacunosum moleculare layer, where they innervate the dendrites of CA1 pyramidal neurons (27). Upon excitation by CA1 pyramidal neurons, OLM neurons release the inhibitory neurotransmitter GABA to the distal dendrites of these CA1 pyramidal neurons,

Significance

Memory formation is a complex process that involves information transfer to the hippocampus for temporary storage (i.e., encoding) and the reciprocal circuit that relays the temporary information back to the neocortex for long-term storage (i.e., consolidation). Acetylcholine has been shown to play a critical role in memory function by differentially modulating encoding and consolidation, but the underlying mechanism is yet unclear. We found that acetylcholine suppresses the hippocampus–entorhinal cortex pathway, which is the gateway to the consolidation pathway. We show that this inhibition is mediated by oriens lacunosum moleculare interneurons and that the ablation of these interneurons impairs proper memory encoding. We provide evidence that demonstrates how acetylcholine tones down the memory consolidation pathway for efficient memory encoding.

Author contributions: J.H., G.C., and J.L.Y. designed research; J.H. and J.Z. performed research; J.H. analyzed data; and J.H., J.Z., G.C., and J.L.Y. wrote the paper.

The authors declare no conflict of interest.

This article is a PNAS Direct Submission.

[1]To whom correspondence should be addressed. Email: yakel@niehs.nih.gov.

This article contains supporting information online at www.pnas.org/lookup/suppl/doi:10.1073/pnas.1712538115/-/DCSupplemental.

opposing excitatory inputs from the temporoammonic pathway (28, 29). Interestingly, it has been shown that OLM interneurons receive heavy cholinergic inputs from the medial septum (30–32), indicating that interneurons may play a critical role in ACh-mediated regulation of the hippocampal output.

In the present study, using slice electrophysiology, optogenetics, and rabies virus-based monosynaptic tracing, we measured synaptic currents and firing activity in CA1 and EC neurons to understand the mechanism of cholinergic modulation of the CA1–EC circuit. We demonstrate here that ACh, by acting on OLM interneurons, increases dendritic inhibition onto CA1 pyramidal neurons and opposes the excitatory temporoammonic inputs, resulting in a decrease in hippocampal output to the EC. In addition, we examined the cholinergic modulation of the circuit by measuring real-time neuronal activity of deep-layer EC neurons in freely moving mice using fiber photometry in combination with optogenetics and pharmacology. Furthermore, we show here, using cell type-specific expression of diphtheria toxin A (DTA) and mouse behavioral testing, that the negative-feedback inhibition is critical for proper memory formation.

Results

Cholinergic Regulation of Hippocampal Output to the EC. We first sought to investigate how medial septum cholinergic neurons, which provide the major cholinergic inputs to the hippocampus (33, 34), influence the hippocampal output to the EC. Previously it has been shown that the hippocampus provides the major input to the deep-layer EC (35). To identify hippocampal neurons that directly project to the EC principle neurons, we used the rabies virus-based monosynaptic tracing method, which allowed us to label presynaptic neurons that synapse onto particular neurons of interest (i.e., principle neurons in the deep-layer EC) (36). To limit the transsynaptic activity of rabies virus to only one synapse without permitting it to cross multiple synapses and spread to other upstream neurons, we used the pseudotyped glycoprotein-deleted rabies virus. This rabies virus can bind only to avian tumor virus receptor A (TVA) receptor-expressing cells and cannot cross any synapse unless rabies glycoprotein B19 is already expressed in the cell (37). We expressed the glycoprotein B19 and TVA in principle neurons in the deep-layer EC by injecting the helper adeno-associated virus (AAV) carrying B19, TVA, and GFP under the CaMKIIα promoter (AAV9-CaMKIIα-DIO-GFP-TVA-B19G) into layer V in the EC (ECV). After 2–4 wk of incubation, during which the TVA receptor and glycoprotein are expressed at a sufficient level for the rabies virus to bind and spread retrogradely by crossing one synapse, we injected rabies virus that carries EnvA and mCherry (EnvA G-deleted rabies-mCherry) into the same site. As the rabies virus was pseudotyped with EnvA, the virus would specifically bind to TVA-expressing cells, targeting only the principle cells in the EC that were previously infected with the helper AAV. As such, the rabies-infected cells would express both GFP and mCherry, whereas the presynaptic cells that project to the rabies-infected cells would express mCherry without GFP expression. We observed cells that were positive for both GFP and mCherry in the EC, where the rabies virus successfully infected TVA-expressing cells (Fig. 1*A*, *Upper*). In the hippocampus, we observed mCherry-positive but GFP-negative cells in the pyramidal layer of the hippocampal area CA1, indicating that these neurons are presynaptic to the principle neurons in the deep-layer EC (Fig. 1*A*, *Lower*). A majority of the mCherry-positive cells were concentrated in the proximal CA1 area, although a few neurons were also found in the CA2 and CA3 areas.

We then examined how cholinergic neurons modulate the excitability of hippocampal area CA1 to the EC circuit using slice electrophysiology. Previously, cholinergic modulation of hippocampal circuits had been examined using acutely prepared transverse or horizontal hippocampal slices that contain cholinergic projections without the cell bodies (15–17, 38–41). However, recent studies have indicated that severed axons may contain down-regulated vesicle clustering compared with those still attached to the cell bodies (42, 43). Furthermore, optogenetic stimulation of axonal terminals, instead of the soma, can produce neurotransmitter release that is not physiologically relevant (44, 45). Therefore, we used the septo-hippocampal coculture system in which a slice containing the medial septum was cocultured adjacent to a hippocampal/EC slice for 2 wk, during which hippocampal neurons guide cholinergic fibers by releasing nerve growth factor (NGF) (46–48). Previous studies have shown that the cholinergic innervation of the target hippocampal neurons in the coculture system is comparable to that observed in vivo (49–51).

Cholinergic neurons specifically express choline acetyltransferase (ChAT), an enzyme that synthesizes ACh. We used the optogenetic technique, which takes advantage of the expression of the light-sensitive receptors opsins in a cell type-specific manner. The light-activated opsin channelrhodopsin-2 (ChR2) was specifically expressed in cholinergic neurons by injecting the Cre-inducible AAV vector carrying ChR2 [AAV-EF1a–double-floxed hChR2 (H134R)–mCherry–WPRE–HGHpA] into the medial septum of cocultured slices from *ChAT-IRES-Cre* mice. We detected mCherry-positive cell bodies of cholinergic neurons in medial septal slices, which project to the hippocampal slices (Fig. 1*B*, *Right*). We used optogenetic stimulation, instead of inhibition, of cholinergic neurons for these in vitro experiments, as cholinergic neurons in slices have low basal activity due to a lack of stimulatory extrinsic inputs that they would receive in vivo during active memory encoding.

We first recorded the firing activity of principal neurons in ECV using loose-seal cell-attached recordings to examine whether cholinergic inputs affect hippocampal theta modulation of ECV neurons. Pyramidal neurons in hippocampal area CA1 are the main output neurons of the hippocampus, as shown in our rabies-tracing results. To mimic theta activity in the CA1 area, the CA1 pyramidal layer was electrically stimulated at a theta frequency using a stimulating electrode (Fig. 1*B*). We found that theta-frequency stimulation (TFS) of the CA1 pyramidal neurons caused an increase in the firing activity in ECV neurons [from 0.10 ± 0.07 to 8.14 ± 3.52 Hz, $n = 11$ neurons, $t(14) = 2.699$, $P = 0.0343$, two-way ANOVA followed by Sidak's multiple-comparisons test] (Fig. 1 *C* and *D*). When cholinergic neurons were stimulated optogenetically with blue light at the beginning of the TFS, the TFS in the CA1 no longer caused a significant increase in the firing in ECV neurons [from 0.14 ± 0.14 to 1.33 ± 0.49 Hz, $n = 5$ neurons, $t(14) = 0.2694$, $P = 0.9565$, two-way ANOVA followed by Sidak's multiple-comparisons test] (Fig. 1 *C* and *D*). These results suggest that cholinergic neurons suppress the excitability of the hippocampus–ECV circuit.

To understand the mechanism underlying this modulation, we examined synaptic transmission from CA1 to the EC. We examined glutamate release from CA1 pyramidal neurons onto ECV neurons by recording evoked excitatory postsynaptic currents (eEPSCs) in ECV neurons upon electrical stimulation of CA1 pyramidal neurons (Fig. 1*B*). The ChR2-expressing cholinergic neurons were photostimulated continuously for ≥350 ms, beginning at least 200 ms before electrical stimulation of CA1 pyramidal layer. When cholinergic neurons were photostimulated, the amplitude of eEPSCs in ECV was significantly smaller than without photostimulation of cholinergic neurons [a 39.2 ± 4.4% decrease compared with control, $n = 10$ neurons, $t(17) = 4.198$, $P = 0.0018$, repeated-measures two-way ANOVA followed by Sidak's multiple-comparisons test] (Fig. 1 *E* and *F*), suggesting a direct role for cholinergic neurons in the regulation of synaptic transmission from the hippocampus to the EC. The ACh effect on eEPSC amplitude was blocked by the $GABA_A$ receptor antagonist gabazine (10 μM), which suggests that the modulation is mediated by GABAergic neurons [in gabazine, 100.3 ± 0.9% of control, $n = 3$ neurons, $t(17) = 0.2074$, $P = 0.9958$, repeated-measures two-way ANOVA followed by Sidak's

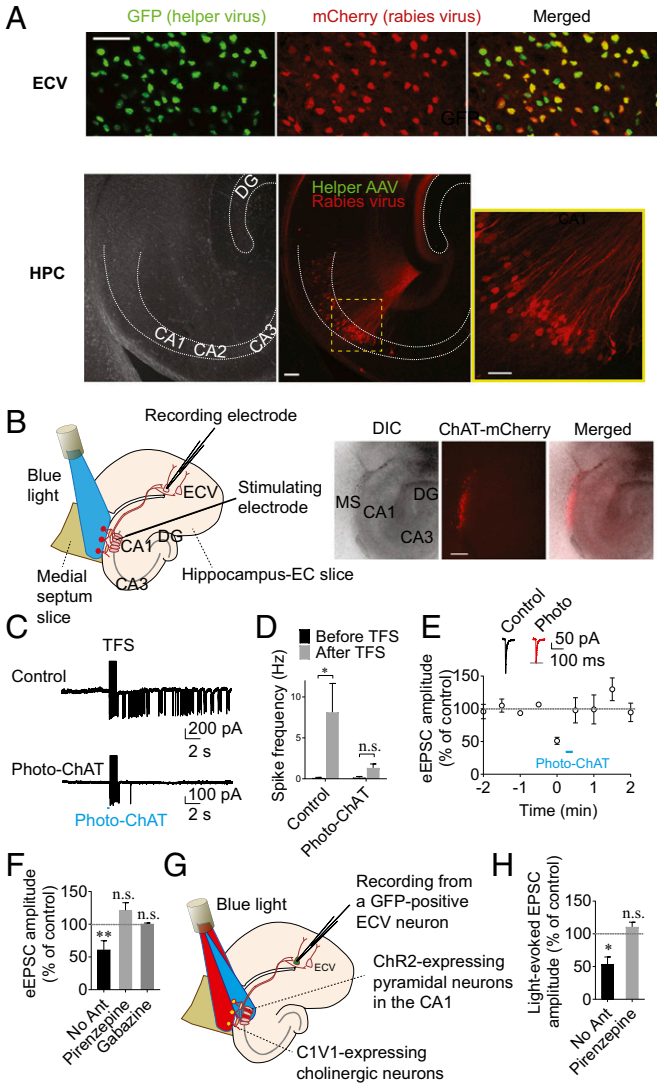

Fig. 1. Cholinergic regulation of the CA1–EC circuit. (*A*, *Upper*) In the ECV, we observed cells that are positive to both GFP and mCherry, suggesting that the cells infected with the helper AAV were successfully targeted by the G-deleted rabies virus. (Scale bar: 50 μm.) (*Lower*) In the hippocampus (HPC), cells that were positive to mCherry but negative to GFP were found in the CA1 pyramidal layer, suggesting that the mCherry-positive cells are presynaptic to the helper AAV-infected cells. DG, dentate gyrus. (Scale bars: 100 μm for low magnification and 50 μm for high magnification.) (*B*) Spike currents were recorded in ECV neurons upon electrical stimulation of CA1 pyramidal neurons to see whether the spiking activity is modulated by photostimulation of cholinergic neurons. (*Left*) A schematic drawing of electrode implantation and blue-light illumination. The ChR2-expressing cholinergic neurons were stimulated with blue light (470 nm, 0.3–2.7 mW) projecting from the 4× objective lens continuously for 350 ms, beginning 200 ms before the first electrical stimulation of the CA1 pyramidal layer. (*Right*) The images of cocultured slices show mCherry-positive, ChR2-expressing cell bodies in the medial septal slice. DIC, differential interference contrast. MS, medial septum. (Scale bar: 300 μm.) (*C*) TFS in the CA1 pyramidal layer caused an increase in spike frequency in ECV neurons (*Upper*), which was blocked by photostimulation of cholinergic (ChAT-positive) neurons (*Lower*). (*D*) Summary bar graph showing the CA1-TFS–induced increase in spike frequency, which was blocked by photostimulation of ChAT neurons. (*E*) Cholinergic modulation of eEPSCs as shown in *B* in ECV was examined. The ChR2-expressing cholinergic neurons were stimulated with blue light (470 nm) continuously for ≥350 ms, beginning at least 200 ms before electrical stimulation of CA1 pyramidal layer. The time course of mean normalized eEPSC amplitude showing the cholinergic suppression of eEPSC amplitude in ECV neurons. Representative traces showing that photostimulation of ChAT neurons (Photo-ChAT) causes a decrease in the amplitude of eEPSCs in an ECV neuron. (*F*) Summary of ACh-induced decrease in eEPSC amplitude, which was blocked by pirenzepine or gabazine. (*G*) Cholinergic modulation of eEPSCs in ECV was examined using the monosynaptic tracing method. In this experiment, CA1 pyramidal neurons that were presynaptic to ECV neurons expressed ChR2 and were stimulated with blue light, whereas ChAT neurons expressed the red-shifted opsin C1V1 and were stimulated by red light. For the stimulation of C1V1-expressing cholinergic neurons, red light (565 nm, 59–352 μW) was applied continuously to the medial septum for at least 300 ms before blue light stimulation (470 nm, 0.15–2.7 mW, 5–10 ms pulse) of the CA1 pyramidal layer. (*H*) Summary bar graph showing that stimulation of cholinergic neurons caused a decrease in light-evoked EPSC amplitude in ECV neurons, which was blocked by pirenzepine. $*P < 0.05$; $**P < 0.01$. n.s., not significant.

multiple-comparisons test] (Fig. 1*F*). Furthermore, we found that the cholinergic suppression of the CA1-evoked eEPSC is mediated by M1 AChRs, as they were blocked by the M1 AChR antagonist pirenzepine [in pirenzepine, 121.4 ± 4.4% of control, $n = 7$ neurons, $t(17) = 2.001$, $P = 0.1738$, repeated-measures two-way ANOVA followed by Sidak's multiple-comparisons test] (Fig. 1*F*).

Given that electrical stimulation of the CA1 pyramidal layer activates all neighboring cells without cell-type specificity, we next aimed to specifically stimulate the CA1 neurons that project to ECV neurons. To do so, we again used the rabies virus-based monosynaptic retrograde tracing method, which allows expression of the blue light-sensitive ChR2 specifically in CA1 pyramidal neurons that are presynaptic to ECV neurons (52). In this way, eEPSCs recorded from ECV neurons can be evoked with blue light stimulation (5–10 ms) of presynaptic CA1 pyramidal neurons instead of electrical stimulation in the CA1 pyramidal layer (Fig. 1*G*). To avoid cross-activation of cholinergic neurons by the same wavelength of light, the red-shifted opsin C1V1 (53) was expressed in cholinergic neurons for this experiment. Furthermore, we used a digital micromirror device to illuminate a spatially defined area of the brain slices. To stimulate CA1 pyramidal neurons, we selectively illuminated the pyramidal layer region in the hippocampus with blue light, whereas the medial septum region was selectively illuminated with red light for the stimulation of cholinergic neurons. As C1V1 is not significantly expressed in the axon terminals (54, 55), the blue light-stimulation of the CA1 pyramidal layers is unlikely to stimulate cholinergic fibers. Similar to our results with the electrically evoked EPSCs, we found that the stimulation of cholinergic neurons (via red light in the medial septal slice just before the blue light stimulation of the CA1 pyramidal layer) caused a decrease in the amplitude of blue light-evoked EPSCs recorded from ECV neurons [50.8 ± 11.0% of control, $n = 8$ neurons, $t(11) = 3.321$, $P = 0.0136$, repeated-measures two-way ANOVA followed by Sidak's multiple-comparison test] (Fig. 1*H*). The cholinergic suppression of CA1-evoked EPSCs was also blocked by pirenzepine [in pirenzepine, 114.4 ± 5.5% of control, $n = 5$ neurons, $t(11) = 0.6068$, $P = 0.8031$, repeated-measures two-way ANOVA followed by Sidak's multiple-comparisons test] (Fig. 1*H*), indicating that the suppression is dependent on M1 AChRs, consistent with our electrically evoked EPSC results (Fig. 1*F*). Together, these results indicate that cholinergic neurons effectively inhibit the hippocampal output to the EC via activating M1 AChRs.

OLM Neurons Modulate the Hippocampal Output to the EC. The finding that the cholinergic suppression of the CA1–EC circuit is blocked by a $GABA_A$ receptor antagonist (Fig. 1*F*) suggests that the modulation is mediated by GABAergic neurons. OLM interneurons are negative-feedback interneurons that innervate the CA1 pyramidal neurons and have been shown to be sensitive to ACh (30, 31). Therefore, we investigated if OLM interneurons mediate the cholinergic suppression of the hippocampal output

to the EC. We first examined whether optogenetic stimulation of cholinergic neurons can induce excitation of OLM interneurons. We recorded AChR current in identified OLM interneurons and investigated whether it can alter the firing of these neurons using whole-cell patch-clamp recordings in the septo-hippocampal coculture system. OLM interneurons were identified based on morphology (i.e., a spindle-shaped cell body horizontally oriented along the pyramidal layer) as well as location (cell body located in the stratum oriens). In addition, OLM interneurons were also identified based on electrophysiological characteristics; the interneurons exhibit prominent sag following hyperpolarization and a sawtooth-shaped firing pattern due to the presence of the hyperpolarization-activated cation current (h-current) (56, 57). To minimize the desensitization of AChRs, we used a short (≤10 ms), single pulse of light to induce ACh release. ACh-induced synaptic currents in OLM interneurons were recorded with whole-cell patch-clamp recordings in the presence of the glutamate receptor antagonists DNQX (20 μM) and AP5 (50 μM) and gabazine (10 μM) to block glutamatergic and GABAergic synaptic currents, respectively (Fig. 2 *A* and *B*). Photostimulation of cholinergic neurons evoked slow inward AChR currents in 93% of OLM interneurons (13 of 14 cells), which were completely blocked by the selective M1 muscarinic AChR antagonist pirenzepine (control, −318,840 ± 84,132 pA/ms; in pirenzepine, 4,062 ± 10,450 pA/ms; $n = 13$ neurons, rank sum difference = −10.88, $P = 0.0014$, rank sum test followed by Dunn's multiple-comparisons test) (Fig. 2 *B–D*). In 57% of OLM cells recorded (8 of 14 cells), optical stimulation of cholinergic neurons evoked fast inward AChR currents, which were blocked by the α7 nicotinic AChR (nAChr) antagonist methyllycaconitine (MLA) but not by pirenzepine, indicating that the fast component is mediated by α7 nAChRs (control, −871.3 ± 562.0 pA/ms; in pirenzepine, −1,221.0 ± 822.1 pA/ms; MLA/pirenzepine, 0.4 ± 4.0 pA/ms; pirenzepine vs. MLA/pirenzepine, rank sum difference = −11, $P = 0.0045$, $n = 6$ neurons, rank sum test followed by Dunn's multiple-comparisons) (Fig. 2 *C* and *E*). All cells that exhibited fast α7 AChR currents also exhibited slow M1 AChR currents. In these α7- and M1-exhibiting cells, the M1 AChR-mediated slow component, due to its slow decay time, accounted for the majority of the total charge (98.9 ± 0.9% of the total area) (Fig. 2*F*). To examine whether the membrane depolarization caused by AChR activation increases the firing activity in OLM interneurons, we performed whole-cell current-clamp recordings. Photostimulation of cholinergic neurons caused a significant increase in spiking activity in OLM neurons (from 0.66 ± 0.18 to 2.4 ± 0.72 Hz, q = 6.002, $P = 0.0295$, $n = 6$ neurons, Tukey's multiple-comparisons test following repeated-measures two-way ANOVA), which was mediated by the M1 muscarinic AChR, as this effect was blocked by pirenzepine (from 0.59 ± 0.12 to 0.50 ± 0.12 Hz, q = 0.3044, $P = 0.9960$, $n = 6$ neurons, Tukey's multiple-comparisons test following repeated-measures two-way ANOVA) (Fig. 2 *G* and *H*). The pirenzepine application did not cause a significant change in the baseline frequency (0.66 ± 0.18 vs. 0.59 ± 0.12, q = 0.2378, $P = 0.9981$, $n = 6$ neurons). The interaction between two factors was significant [$F(1, 5) = 9.942$, $P = 0.0253$, repeated-measures two-way ANOVA]. These data indicate that the stimulation of cholinergic neurons causes membrane depolarization in OLM interneurons and increases the firing rate of these neurons via M1 muscarinic AChRs.

Cholinergic Neurons Decrease the Firing Rate of CA1 Pyramidal Neurons. OLM interneurons are GABAergic interneurons that release the inhibitory neurotransmitter GABA onto dendrites of CA1 pyramidal neurons upon excitation. Cholinergic activation of OLM interneurons should stimulate GABA release onto CA1 pyramidal neurons. Therefore, we recorded inhibitory postsynaptic currents (IPSCs) in the somata of CA1 pyramidal neurons in the presence of the glutamate receptor antagonists

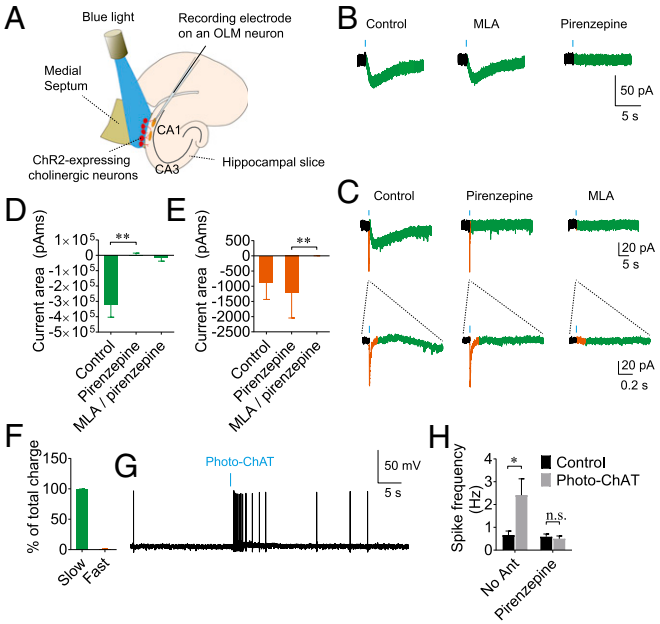

Fig. 2. Cholinergic activation of OLM interneurons. (*A*) A schematic showing recording of AChR currents in OLM interneurons triggered by photostimulation of cholinergic neurons. (*B*) Photostimulation of cholinergic neurons (shown as blue bars, 0.27–2.7 mW LED on cholinergic cell bodies through the 4× objective or 60–600 μW LED light onto the cholinergic fibers through the submerged 40× objective) for 1–10 ms evoked slow inward currents (green) in the majority of OLM interneurons (~93%). (*C*) In a subset of OLM cells recorded (~60%), ACh also evoked fast inward currents (orange), which were sensitive to the α7 nAChR antagonist MLA but not to pirenzepine. (*D*) Average areas of slow currents evoked by photostimulation of cholinergic neurons, showing that the slow currents are mediated by the M1 muscarinic AChRs. (*E*) Average areas of fast currents evoked by photostimulation of cholinergic neurons showing that the fast currents are mediated by α7 nAChR and are blocked by MLA. (*F*) Summary bar graph showing the contributions of fast and slow components to the total charge. (*G*) A representative current-clamp recording trace showing that photostimulation of ChAT neurons caused an increase in spike frequency in OLM neurons. (*H*) Summary bar graph showing an increase in spike frequency induced by cholinergic neurons, which was abolished in the presence of pirenzepine. *$P < 0.05$; **$P < 0.01$.

DNQX and AP5. In parallel with our data that show an increase in spiking in OLM neurons (Fig. 2 *G* and *H*), photostimulation of cholinergic neurons caused an increase in IPSC frequency in CA1 pyramidal neurons [from 6.0 ± 0.8 to 13.1 ± 1.4 Hz, 173.2 ± 37.3% increase in IPSC frequency, $n = 14$, $t(25) = 6.553$, $P < 0.0001$, two-way ANOVA followed by Sidak's multiple-comparisons test] (Fig. 3 *A* and *B*), demonstrating an increase in GABAergic transmission to these neurons. The ACh-induced increase in IPSC frequency was blocked by pirenzepine [14.8 ± 7.4% increase, $n = 4$ neurons, $t(25) = 0.7918$, $P = 0.8205$] and by the broad-spectrum muscarinic AChR antagonist atropine [10.4 ± 12.3% increase, $n = 10$ neurons, $t(25) = 0.7321$, $P = 0.8519$], suggesting that the synaptic modulation is mediated by M1 muscarinic AChRs (Fig. 3*C*), consistent with cholinergic modulation of spiking in OLM interneurons (Fig. 2*H*). In contrast, the selective α7 nAChR antagonist MLA did not block the cholinergic stimulation of IPSCs (Fig. S1), suggesting that the cholinergic stimulation of GABAergic transmission is not dependent on the α7 nAChRs.

Changes in local inhibitory feedback input effectively modulate the firing activity of neurons, as shown in vitro and in vivo in many parts of the brain (58, 59). Therefore, we examined whether cholinergic activation of OLM interneurons regulates the firing activity of CA1 pyramidal neurons. Without activation

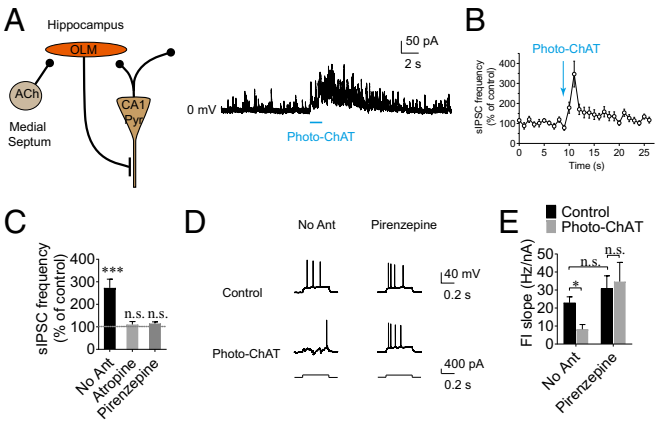

Fig. 3. Cholinergic regulation of CA1 pyramidal neurons. (*A*) Photostimulation (488-nm laser, 20–100 uW delivered through the 5× objective lens for 0.9–1.4 s) of ChAT neurons caused an increase in IPSC frequency in CA1 pyramidal neurons. (*B*) Time course of mean normalized frequencies of IPSCs showing the effect of photostimulation of cholinergic neurons on IPSC frequency in CA1 pyramidal neurons. (*C*) Summary of mean normalized IPSC frequencies. Photostimulation of cholinergic neurons caused a significant increase in IPSC frequency, which was blocked by atropine or pirenzepine. See also Fig. S1. (*D*) Representative traces showing that photostimulation of ChAT neurons caused a decrease in depolarization-induced spiking in CA1 pyramidal neurons, which was abolished in the presence of pirenzepine. The septum and stratum oriens were illuminated by the blue LED light (470 nm, 0.6–2.77 uW) for a total of 800 ms beginning 400 ms before the 400-ms depolarizing step. (*E*) Summary of F/I slope showing a decrease in F/I slope induced by cholinergic neurons, which was blocked by pirenzepine. $*P < 0.05$; $***P < 0.001$.

of cholinergic circuits, application of a short positive-current pulse to CA1 pyramidal neurons induced membrane depolarization and firing of these neurons in current-clamp recordings. (Fig. 3*D*). However, when cholinergic neurons were optogenetically activated, CA1 pyramidal cells fired at a significantly lower frequency in response to the same magnitude of depolarizing pulse (Fig. 3*D*). As such, activation of cholinergic circuits caused a decrease in the frequency–current (F/I) slope in CA1 pyramidal neurons (from 22.9 ± 2.7 to 8.2 ± 2.6 Hz/nA, n = 6 neurons, q = 6.055, $P = 0.0285$, Tukey's multiple-comparisons test following repeated-measures two-way ANOVA) (Fig. 3*E*), indicating that cholinergic potentiation of negative-feedback inhibition of CA1 pyramidal neurons effectively suppresses the firing output of these neurons. The ACh-induced decrease in F/I slope was blocked by pirenzepine, indicating that the modulation is mediated by M1 muscarinic AChRs (from 31.0 ± 6.9 to 34.7 ± 10.7 Hz/nA, n = 6 neurons, q = 1.531, $P = 0.7139$, Tukey's multiple-comparisons test following repeated-measures two-way ANOVA) (Fig. 3*E*), consistent with our finding that M1 AChRs mediate cholinergic suppression of hippocampal output to the EC (Fig. 1 *F* and *H*) and activation of OLM interneurons (Fig. 2*H*). The pirenzepine application did not cause a significant change in the baseline frequency (22.88 ± 2.73 vs. 30.97 ± 6.91 Hz/nA, q = 3.342, $P = 0.2026$, n = 6 neurons). The interaction between the two factors was significant [$F(1, 5) = 14.39$, $P = 0.0127$, repeated-measures two-way ANOVA].

We also tested whether direct stimulation of OLM interneurons is capable of suppressing the hippocampal output to the EC. OLM interneurons are a subset of somatostatin-expressing neurons in the hippocampus and account for the majority of somatostatin-expressing neurons located in the stratum oriens (28, 60). To express the blue light-sensitive ChR2 specifically in somatostatin neurons, the Cre-inducible AAV vector carrying ChR2 was injected into cultured slices from the somatostatin-specific Cre line *Som-IRES-Cre* mice. To specifically stimulate somatostatin-expressing neurons in the stratum oriens, we selectively illuminated the deeper portion of the stratum oriens with the digital micromirror device (Fig. S2*A*). Photostimulation of OLM interneurons caused a significant decrease in CA1-evoked eEPSC amplitude in ECV neurons (21.5 ± 8.7% of control) (Fig. S2 *B* and *C*), which was consistent with the effect of photostimulation of cholinergic neurons. In fact, the photostimulation of OLM neurons caused a larger effect on eEPSCs in ECV neurons than that caused by photostimulation of ChAT neurons, perhaps because the photostimulation causes more robust activation of OLM neurons than AChR activation of these neurons. The OLM neuron-mediated decrease in eEPSC was blocked by gabazine, indicating that the effect requires GABAergic transmission (99.8 ± 3.4% of control) (Fig. S2*C*). These data demonstrate that OLM interneurons inhibit the hippocampal output to the EC.

Cholinergic Regulation of Deep-Layer EC Neurons. We next investigated whether the cholinergic modulation of hippocampal output to the EC occurs in vivo. To examine the activity of the EC neurons in freely moving mice, we used fiber photometry (Fig. 4*A*), which can detect population activity of principal neurons in deep brain regions (61). To monitor the activity of principal neurons in the deep-layer EC, we expressed the calcium indicator GCaMP6f by stereotaxically injecting AAV carrying GCaMP6f under the glutamatergic neuron-specific promoter CaMKIIα into the deep layer of the EC (Fig. 4*B*). As a control fluorescence signal, AAV carrying the RFP tdTomato was coinjected with the AAV carrying GCAMP6f (Fig. 4*B*). Optical probes implanted into the deep-layer EC neurons were used to deliver excitation light at 488 nm into the brain region and acquire real-time readouts of fluorescent signals (Fig. S3). Any fluctuations in fluorescence signal caused by an animal's movements and/or changes in the connection between the photon detector and the optical fiber would manifest in both GCaMP6f and tdTomato signals (Fig. 4*C*), both of which were acquired through the same optical implant and patch cable. As such, by taking the ratiometric measurement, signal artifacts can be eliminated; thus, the intracellular calcium signal is represented as the ratio of the GCamp6f signal to the tdTomato signal (Fig. 4*C*, *Lower*). Spontaneous calcium transients of a low frequency (0.63 ± 0.15 Hz) were observed in deep-layer EC in freely moving mice placed in a novel environment (Fig. 4*E*, *Upper*). Levels of ACh in the hippocampus are high during active memory encoding but low during slow-wave sleep, when memory consolidation is dominant (6, 10, 11). Therefore, we investigated how the blockade of cholinergic neurons modulates the deep-layer EC neurons in awake animals. To specifically inhibit medial septal cholinergic neurons, we used optogenetics to specifically inhibit the medial septal cholinergic neurons in vivo with light (Fig. 4*A*). The light-activated inhibitory opsin archaerhodopsin-3 (Arch) was expressed in cholinergic neurons in the medial septum (Fig. 4*D*) by stereotaxically injecting the Cre-inducible AAV vector carrying double-floxed Arch (AAV-FLEX-Arch-GFP) into the medial septum of *ChAT-IRES-Cre* mice. The medial septal region, where cholinergic cell bodies are located, was illuminated continuously for 10 min with green light (561 nm) to prevent rebound excitation of the Arch-expressing cells. Optogenetic inhibition of the cholinergic neurons caused an increase in the activity of principle neurons in the deep-layer EC as evidenced by a significant increase in the calcium transient frequency [from 34.3 ± to 45.6 ± 8.7 transients/min; n = 5 mice, $t(4) = 4.582$, $P = 0.0102$, Student's paired t test] (Fig. 4 *E*–*G*). The fact that the inhibition of cholinergic neurons causes an increase in the activity of principle neurons in the deep-layer EC neurons suggests that septal cholinergic neurons actively inhibit the neuronal activity in the EC neurons when animals are awake and freely moving. We further tested whether the pharmacological

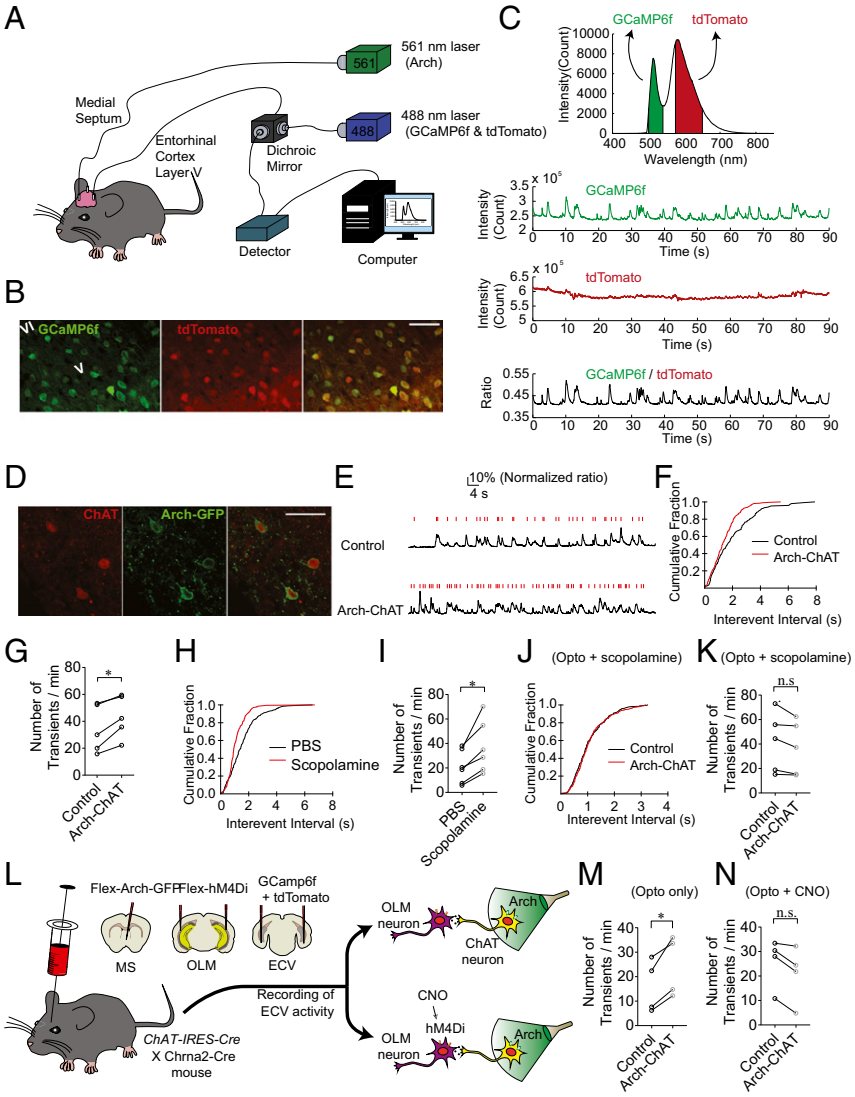

Fig. 4. Cholinergic suppression of entorhinal cortical neurons in vivo. (*A*) A schematic drawing showing the photometry setup to examine population activity of EC neurons in freely moving mice. (*B*) GCaMP6f (calcium indicator) and tdTomato (control fluorescent protein) expression in the deep-layer EC showing colocalization of the fluorophores. (Scale bar: 50 μm.) (*C*) GCaMP6f and tdTomato signals were obtained from the same optical fiber; unlike the GCaMP6f signal, the tdTomato signal was steady without showing transients. The ratio of the GCaMP6f signal to the tdTomato signal was taken as a measure of calcium signals. (*D*) Arch-GFP and ChAT expression in the medial septum showing that cholinergic neurons expressed Arch-GFP. (Scale bar: 50 μm.) (*E*) Representative traces showing that photoactivation of Arch in ChAT neurons (Arch-ChAT) causes an increase in the transient frequency. (*F*) Cumulative Kolmogorov–Smirnov plots of transient intervals from the traces shown in *D* exhibited a shift toward shorter interevent intervals during optogenetic inhibition of ChAT neurons. (*G*) Optogenetic inhibition of ChAT neurons caused a significant increase in transient frequency in the deep layer EC. (*H*) Cumulative Kolmogorov–Smirnov plots of transient intervals showed a shift toward shorter interevent intervals with i.p. scopolamine administration. (*I*) The pharmacological blockade of muscarinic AChRs by scopolamine caused a significant increase in transient frequency in the deep-layer EC. (*J*) Cumulative Kolmogorov–Smirnov plots of transient intervals showed no change in the response to optogenetic inhibition of cholinergic neurons when scopolamine was preapplied. (*K*) Summary graph showing that preapplication of scopolamine occluded the increase in transient frequency in the deep-layer EC induced by optogenetic inhibition of ChAT neurons. (*L*) The inhibitory opsin was specifically expressed in cholinergic neurons in the medial septum, whereas the inhibitory DREADD hM4Di was specifically expressed in OLM interneurons. For photometry recordings, GCamp6f and tdTomato were expressed in the deep-layer EC as shown in Fig. 1*B*. Cholinergic modulation of ECV activity was examined with or without CNO application. (*M*) Without CNO application, optogenetic inhibition of septal cholinergic neurons caused a significant increase in calcium transients in the deep-layer EC. (*N*) When CNO was administered for chemogenetic inhibition of OLM interneurons, optogenetic inhibition of septal cholinergic neurons no longer caused a decrease in transients in the deep-layer EC. *$P < 0.05$.

blockade of muscarinic AChRs induces a similar response. I.p. injection of the muscarinic AChR antagonist scopolamine (1 mg/kg body weight) caused a significant increase in the calcium transient frequency [from 21.0 ± 5.6 to 37.1 ± 8.7 transients/min; n = 6 mice, $t(5) = 4.078$, $P = 0.0096$, Student's paired t test] (Fig. 4 *H* and *I*). In addition, preapplication of scopolamine not only caused a significant increase in transient frequency in the deep-layer EC but also occluded the increase caused by optogenetic inhibition of cholinergic neurons [from 41.4 ± 11.0 to 36.7 ± 9.9 transients/min, $n = 5$ mice, $t(4) = 2.369$, $P = 0.0797$, Student's paired t test] (Fig. 4 *J* and *K*), suggesting that the cholinergic regulation of EC activity is dependent on muscarinic AChRs.

We next investigated whether the cholinergic suppression of the deep-layer EC activity that we observed in vivo is mediated by OLM interneurons. We therefore tested whether optogenetic inhibition of septal cholinergic can still increase neuronal activity

in the deep-layer EC neurons when OLM interneurons are chemogenetically inhibited. To express the clozapine-*N*-oxide (CNO)-activated inhibitory designer receptors exclusively activated by designer drugs (DREADDs) (62) specifically in OLM interneurons, we used the OLM-specific α2 nAChR (Chrna2)-Cre mouse line (28, 63). It should be noted that we could not use the *Som-IRES-Cre* mouse line for these in vivo studies as we did for our in vitro studies because the Cre line is not specific to OLM interneurons without limiting the viral solution to the stratum oriens; diffusion of the viral solution to other layers would inadvertently ablate non-OLM interneurons (e.g., Som-expressing neurons in other layers of the hippocampus). We stereotaxically injected the AAV virus carrying Cre-dependent DREADDs [AAV-hSyn-DIO-hM4D(Gi)-mCherry] into the hippocampi of the double-Cre–cross mice which were acquired by crossbreeding *ChAT-IRES-Cre* with Chrna2-Cre mice (Fig. 4*L*). The inhibitory opsin Arch was expressed in septal cholinergic neurons in the medial septum by stereotaxically injecting the Cre-inducible AAV vector carrying double-floxed Arch (AAV-FLEX-Arch-GFP) into the medial septum (Fig. 4*L*), as we did in *ChAT-IRES-Cre* mice (Fig. 4*D*). Without CNO administration, optogenetic inhibition of septal cholinergic neurons caused a significant increase in transients in the deep-layer EC in these mice [from 16.1 ± 5.4 to 24.2 ± 6.2 transients/min, $n = 4$ mice, $t(3) = 4.334$, $P = 0.0225$, Student's paired t test] (Fig. 4*M*), consistent with the data we have shown in *ChAT-IRES-Cre* mice (Fig. 4*G*). When CNO was administered to inhibit OLM interneurons, on the contrary, the optogenetic inhibition of septal cholinergic no longer caused an increase in EC neuron activity (from 25.7 ± 5.1 to 20.8 ± 5.8 transients/min, $n = 4$ mice, $W = -10$, $P = 0.1250$, Wilcoxon matched-pairs signed rank test) (Fig. 4*N*), suggesting that the cholinergic action is mediated by OLM interneurons.

OLM Interneurons Are Critical for Hippocampus-Dependent Memory. Our in vitro slice electrophysiology and in vivo fiber photometry results suggest that negative-feedback inhibition by OLM interneurons plays an important role in mediating ACh modulation of the hippocampal output. To further examine how OLM neurons play a role in memory formation, we conducted mouse behavioral studies whereby we investigated the effect of the ablation of OLM interneurons on hippocampus-dependent and -independent memory function. To specifically ablate OLM interneurons, we used the OLM-specific Chrna2-Cre mouse line (28, 63). Ablation of OLM neurons was achieved by stereotaxically injecting the AAV9 virus carrying Cre-dependent DTA (AAV-mCherry-flex-dtA) into the hippocampi of Chrna2-Cre mice (Fig. S4*A*). DTA expressed in Cre-positive cells blocks protein synthesis, leading to cell death in these neurons. We observed a significant decrease in the number of OLM interneurons in the caudal/ventral hippocampus but not in the rostral/dorsal hippocampus (Fig. S4*C*), which is consistent with previous studies that showed higher expression of Chrna2 in ventral OLM interneurons (64, 65). The Cre-dependent cell ablation was specific to OLM interneurons, without affecting the number of CA1 pyramidal neurons (Fig. S4*D*).

After a minimum 3 wk of recovery following virus injection, we investigated hippocampus-dependent and -independent memory function in the OLM-ablated mice and their littermate controls. The object-location task (OLT) is based on the rodents' inherent curiosity about objects with a novel location and is considered a hippocampus-dependent memory task (66, 67). Mice were placed in an arena with two identical objects during the training phase of the OLT, and one of the objects was moved to a new location during the retention delay of 20 min before the testing phase (Fig. 5*A*). When placed back into the arena during the testing phase, the control mice spent significantly more time with the object that was in a novel location than with the object in a familiar location [stationary object, 23.1 ± 3.0 s vs. displaced object, 35.0 ± 3.2 s, $n = 10$ mice, $t(19) = 3.06$, $P = 0.0128$, two-way ANOVA followed by Sidak's multiple-comparisons test], whereas OLM-ablated mice spent comparable amounts of time with either object [stationary object, 25.6 ± 3.5 s vs. displaced object, 25.1 ± 2.5 s, $n = 11$ mice, $t(19) = 0.135$, $P = 0.9888$, two-way ANOVA followed by Sidak's multiple-comparisons test] (Fig. 5 *B* and *C*).

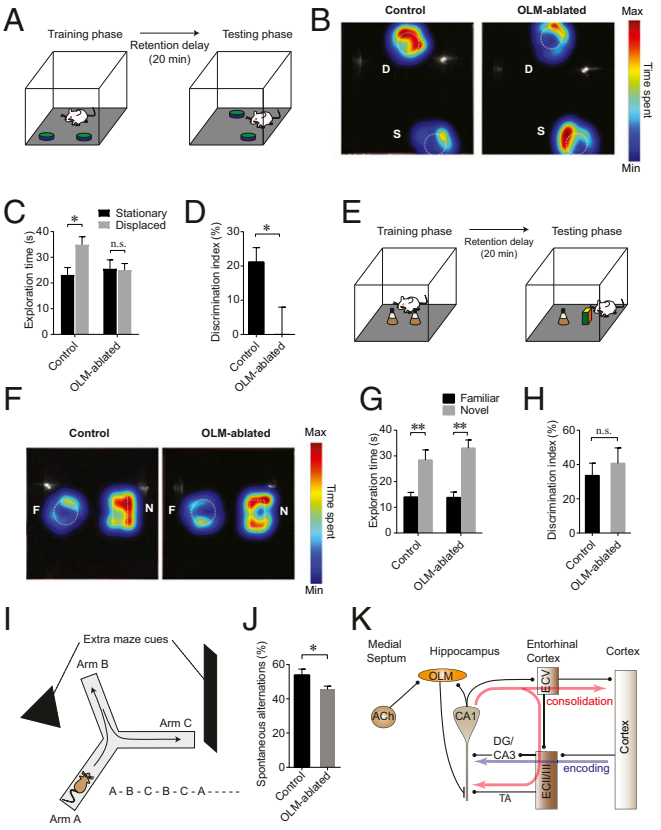

Fig. 5. Ablation of OLM interneurons impairs the encoding of spatial memory. (*A*) A schematic drawing showing the OLT. During the training phase, a mouse was placed in an arena that contained two identical objects. After a 20-min retention delay, during which one of the objects was moved to a new location, the mouse was replaced in the arena, and the mouse's exploration of the objects was recorded. (*B*) Heat maps showing that an OLM-ablated mouse, unlike the control mouse, does not show a preference for the object with a novel location (D, displaced) over the object that has not been moved (S, stationary). (*C*) Summary of exploration time for each object showing that the littermate controls spent significantly more time on the object with a novel location, whereas OLM-ablated mice did not show a preference for the object with a novel location. (*D*) The DI of OLM-ablated mice was significantly lower than that of control mice. (*E*) A schematic drawing showing the NORT. In this task one of the initial objects placed during the training phase was replaced with a novel object before the testing phase. (*F*) Heat maps showing that both control and OLM-ablated mice preferred the novel (N) over the familiar (F) object. (*G*) OLM-ablated mice spent significantly more time on exploring the novel object, as did the control mice. (*H*) Summary bar graph showing that DI of the OLM-ablated mice was not significantly different from that of controls. (*I*) OLM-ablated mice were tested for the spontaneous alternation task on a Y-maze with extramaze spatial cues to determine their spatial working memory. (*J*) OLM-ablated mice showed significantly reduced spontaneous alternation performance compared with their littermate controls. See also Figs. S4–S6. (*K*) A proposed model of cholinergic regulation of the hippocampus–EC circuit. ACh stimulates OLM interneurons in the hippocampus by activating M1 muscarinic AChRs expressed on OLM interneurons. The activation of OLM interneurons causes an increase in GABAergic synaptic inputs to the dendrites of CA1 pyramidal neurons in the stratum lacunosum moleculare layer, which effectively suppresses the temporoammonic (TA) pathway-induced firing of CA1 pyramidal neurons. This suppresses the memory-consolidation circuits (by decreasing output to the ECV), which then may allow CA1 pyramidal neurons to be available for regulation via the memory-encoding pathway. *$P < 0.05$; **$P < 0.01$.

The discrimination index (DI) in OLM-ablated mice was significantly lower than that of the control group, indicating impaired spatial memory [control, 21.17 ± 4.19, n = 10 mice; OLM-abated, 0.06 ± 7.94, n = 11 mice, $t(19) = 2.283$, $P = 0.0341$, Student's unpaired t test] (Fig. 5*D*).

The novel object recognition task (NORT) is similar to the OLT, but instead of one of the objects being moved, one of the objects is replaced (Fig. 5*E*). The NORT without contextual or temporal factors is generally considered a hippocampus-independent memory task (66, 68). In our NORT tests, which did not include a contextual or temporal component, the OLM-ablated mice exhibited preference for the novel over the familiar object [familiar object,13.8 ± 2.2 s vs. novel object, 33.0 ± 3.2 s, n = 6 mice, $t(19) = 4.593$, $P = 0.0015$, two-way ANOVA with Sidak's multiple-comparisons test], as did control mice [familiar object, 14.0 ± 1.8 s vs. novel object, 28.4 ± 3.9 s, n = 7 mice, $t(19) = 3.719$, $P = 0.0068$, two-way ANOVA with Sidak's multiple-comparisons test] (Fig. 5 *F* and *G*). The DI of the OLM-ablated mice was not significantly different from the control group, indicating that they had intact object-recognition memory [control, 33.53 ± 7.29, n = 7; OLM-ablated, 40.70 ± 9.06, n = 6 mice, $t(11) = 0.6225$, $P = 0.5463$, Student's unpaired t test] (Fig. 5*H*).

To further assess the functional specificity of OLM interneurons in memory formation, we investigated whether OLM-ablated mice have intact spatial working memory using the Y-maze. We utilized the Y-maze spontaneous alternation test, which is based on the rodents' innate curiosity to explore more novel spaces; a higher spontaneous alternation rate indicates more intact spatial working memory (Fig. 5*I*). OLM-ablated mice showed reduced spontaneous alternation performance in the Y-maze task compared with their Cre-negative littermates [control, 53.92 ± 3.46%, n = 8 mice; OLM-ablated, 45.51 ± 1.91%, n = 12 mice, $t(18) = 2.298$, $P = 0.0337$, Student's unpaired t test] (Fig. 5*J*), suggesting impaired spatial working memory. Direct (control, 9.1 ± 1.8%; OLM-ablated, 12.5 ± 1.6%) and indirect revisits (control, 24.8 ± 2.7%; OLM-ablated, 27.0 ± 1.5%) in OLM-ablated mice were not significantly different from the control group (Fig. S5). Together, these results indicate a critical role for OLM interneurons in hippocampus-dependent memory, which is impaired when these neurons are ablated. The OLM-ablated mice did not show any significant change in body weight gain, locomotion, or anxiety-related behavior (Fig. S6).

Discussion

A critical role for ACh in memory function has previously been shown in rodents as well as in humans, in which dysfunction of the cholinergic system causes memory impairment (4, 14, 69–73). Using slice electrophysiology, it has been shown that at the circuit level ACh modulates intrinsic connections in the hippocampus (15–17, 38, 40, 41). However, one important remaining question has been whether ACh regulates the hippocampal output to the EC. Using a variety of in vitro and in vivo techniques, we show here that cholinergic neurons in the medial septum suppress the hippocampal output to the deep-layer EC and that this has implications for memory formation.

Given that the hippocampus–EC circuit is the gateway to the memory-consolidation pathway (1, 2, 74), the cholinergic suppression of hippocampal output that we observed is in parallel with the previous studies that show differential effects of ACh on the memory-encoding and -consolidation processes. It has been shown that ACh not only stimulates memory encoding but also suppresses the memory-consolidation process (4, 6, 12–14). This ensures that the memory-encoding and -consolidation pathways are temporally separated, preventing them from interfering with each other (3–7). However, until now it has remained unclear how ACh suppresses the consolidation process. Our data suggest that ACh suppresses the hippocampal output to the EC, the passage to the consolidation pathway, and that this regulation is critical for proper formation of hippocampus-dependent memory.

What is the mechanism that might explain our observation that suppression of the CA1–EC circuit is critical for proper memory formation? As a part of the memory consolidation pathway, ECV neurons project to neurons in the neocortex to convey hippocampal information for the formation of long-term memory, but at the same time these neurons also project to the superficial layer in the EC, which subsequently projects back to the hippocampal area CA1 (25, 26). The recurrent pathway, called the "temporoammonic pathway," has been shown to be critical for memory consolidation (22), allowing the reentrance of the processed information back to the hippocampus. However, given that the same type of neurons (i.e., CA1 pyramidal neurons) also receive the Schaffer collateral inputs as a part of memory-encoding pathway, overactivation of the recurrent pathway (i.e., the ECV–ECIII–CA1 temporoammonic pathway) will interfere with incoming information from the neocortex during encoding. As such, cholinergic suppression of the hippocampal output during encoding might be essential in temporarily separating the recurrent inputs from newly incoming information (Fig. 5*K*).

Additionally, when we further examined the hippocampus–EC circuit using in vitro slice electrophysiology and in vivo photometry recording in combination with optogenetics and chemogenetics, we found that OLM interneurons, which are a negative-feedback regulator, played a critical role in the cholinergic regulation of the informational flow from the hippocampus to the EC. OLM interneurons innervate the distal dendrites of CA1 pyramidal neurons in the stratum lacunosum moleculare, where the temporoammonic pathway from the EC arrives. This anatomical structure allows the OLM interneurons to selectively inhibit the temporoammonic inputs (28). The OLM neuron-mediated negative-feedback mechanism suggests an important aspect of the cholinergic regulation, which is that ACh can selectively tune the temporoammonic pathway-induced firing of CA1 pyramidal neurons without limiting the Schaffer collateral pathway-induced firing. Using behavioral studies, we demonstrated that the negative-feedback inhibition mediated by OLM interneurons plays a critical role in memory encoding. These findings complement previous studies on the firing pattern of OLM interneurons; OLM interneurons fire more actively when an animal is awake and engaged in learning and are suppressed when the animal is asleep or at rest, during which time newly formed memory is consolidated (75, 76). However, the critical role for the OLM in learning has remained unclear until now. Our results demonstrate that OLM interneurons are crucial in the encoding of hippocampus-dependent memory via suppression of the CA1–ECV pathway.

In this study, we found that OLM interneurons in the intermediate/ventral hippocampus play a critical role in the encoding of spatial memory. These results are surprising, given that early anatomical and lesion studies have shown that the dorsal hippocampus is critical for spatial and episodic memory, whereas the ventral hippocampus is involved in emotional behaviors or the stress response. This discrepancy can be explained by the following two reasons. First, it has been shown that each OLM interneuron makes more than 10,000 synaptic boutons in the stratum lacunosum moleculare layer, thereby affecting a large number of CA1 pyramidal neurons (27). As such, OLM interneurons located in the ventral/intermediate hippocampus may affect CA1 pyramidal neurons in the dorsal hippocampus. Second, data from recent studies suggest that the ventral hippocampus is also involved in spatial and contextual memory by interacting with the dorsal hippocampus (77, 78). Cells in the ventral hippocampus, similar to the dorsal hippocampus, fire action potentials when an animal is in a specific field of space,

called "the place field," suggesting a role in spatial processing. The ventral hippocampal neurons, having larger place fields than cells in the dorsal hippocampus (79), have been suggested to play a role in higher-order memory representations (80).

Using in vitro slice electrophysiology, we have shown that photoactivation of either cholinergic or OLM interneurons can effectively control the CA1 output to the EC circuit. It is possible that our optogenetic stimulation activates the neurons differently from the in vivo condition, inducing an unnatural firing frequency or mode of firing. To rule out this possibility, in our in vivo fiber photometry experiments we inhibited the neurons during the condition when cholinergic tone is naturally high; the results showed an increase in EC activity (Fig. 4), consistent with our in vitro observations.

In conclusion, we demonstrate that cholinergic inputs originating from the medial septum effectively suppress the hippocampal output to EC by increasing negative-feedback inhibition through OLM interneurons and that this regulation is critical for hippocampus-dependent memory. Dissection of the cholinergic regulation of the hippocampal circuit and identification of the key players will allow better understanding of cholinergic modulation of memory function. Our results are consistent with findings in humans showing the selective loss of OLM interneurons in age-related cognitive impairments (81) and suggest that this pathway may be a target for therapeutic interventions.

Materials and Methods

Animals. *ChAT-IRES-Cre* and *Som-IRES-Cre* knockin mice were originally obtained from the Jackson Laboratory. The Chrna-cre transgenic mouse line was originally obtained from Mutant Mouse Resource and Research Centers (MMRRC). Three- to ten-month-old male mice were used for fiber photometry recordings, rabies virus-based monosynaptic tracing, and behavioral testing. All animal procedures were performed according to the animal study protocols approved by the National Institute of Environmental Health Sciences Animal Care and Use Committee and in compliance with the NIH Humane Care and Use of Animals regulations.

Details regarding animals can be found in *SI Materials and Methods*.

Monosynaptic Tracing. The AAV helper virus (AAV9-CaMKIIa-T2A-TVA-E2A-B19G) was injected into the ECV of 10- to 12-wk-old *ChAT-IRES-Cre* mice. After a minimum of 4 wk of recovery post AAV virus injection, the attenuated G-deleted rabies virus (EnvA G-deleted Rabies-mCherry) was injected to the ECV. Seven to ten days after the rabies injection, mice were transcardially perfused for immunohistochemical staining. The details of virus injection can be found in *SI Materials and Methods*.

Septo-Hippocampal Coculture System. The coculture was made from 7- to 8-d-old *ChAT-IRES-Cre* mice. A coronal slice containing the medial septum was placed near a horizontal slice containing the hippocampus, which was cultured at least for 2 wk before being used for electrophysiological recordings. Virus was injected into slices using a microinjector through a glass pipette targeting the area of interest. The details of the coculture system and virus injection can be found in *SI Materials and Methods*.

In Vivo Fiber Photometry. A fiber photometry system similar to that previously described (61) was used for in vivo measurements of GCaMP6f fluorescence in ECV neurons. After a minimum of 4 wk of recovery after intracerebral microinjection of the virus, optical probes were implanted in the deep layers of the EC. At least 2 wk of recovery were allowed before in vivo measurement of fluorescence signals. The normalized ratio of GCaMP6f/tdTomato ($R_{G/td}$) was used to represent calcium signals. The details of virus injection, photometry setup, and data analysis can be found in *SI Materials and Methods*.

Electrophysiology. Electrophysiological recordings were performed on a horizontal hippocampal slice. For electrical stimulation, a bipolar stimulating electrode was lowered to the region of interest before recordings. Synaptic currents were recorded at −60 mV using the whole-cell patch-clamp configuration. For recording of spikes, whole-cell current-clamp or loose-seal recordings were used. For loose-seal recordings, spike currents were recorded at the membrane potential with 0 pA current injection. The details of the experiments can be found in *SI Materials and Methods*.

Immunohistochemistry. For tissue collection, mice were transcardially perfused with 4% paraformaldehyde (PFA) in 0.1 M PBS with heparin. The brains were then equilibrated with 30% sucrose and were frozen for cryosection. Sections were then incubated with a primary antibody overnight, which was followed by a 2- to 4-h incubation with a secondary antibody. The sections were imaged on a confocal microscope (Zeiss LSM 710 or LSM 880; Carl Zeiss). The details of immunostaining, imaging, and data analysis can be found in *SI Materials and Methods*.

Behavioral Assays. After virus injection, mice were allowed to recover for at least 3 wk before behavioral testing. Before being tested for the OLT, mice were habituated to the open-field chambers for 3 d for 10 min/d. The mouse's ambulatory distance and time spent in the central zone were recorded during the first day of habituation. During the 10-min training phase, the mouse was placed in the open-field chamber where two identical objects were placed. Mice were placed back in the same arena after a retention delay of 20 min, during which one of the objects was moved to a new location (OLT) or replaced with a novel object (NORT). The DI was calculated as follows: $(T_{novel} - T_{familiar})/(T_{novel} + T_{familiar}) \times 100$. For the Y-maze spontaneous alternation task, mice were placed on a Y-maze for 8 min, during which they were allowed to freely explore the three distal arms. The percent of spontaneous alternations was calculated by dividing the number of alternations by the maximum possible number of alternations as follows: (number of alternations)/(total number of arm entries − 2) × 100. The details of behavioral tests can be found in *SI Materials and Methods*.

Statistics. For comparison of two groups, Student's *t* test and Mann–Whitney *U* test were used. For comparisons of multiple groups, ANOVA and Wilcoxon signed-rank test were used. Pairwise comparisons were performed using Sidak's multiple-comparisons and Tukey's test. The details of statistical tests can be found in *SI Materials and Methods*.

ACKNOWLEDGMENTS. We thank Pattie Lamb for preparing plasmids and genotyping animals; Dr. Negin Martin for rabies virus packaging; Dr. Bernd Gloss for AAV virus packaging; Jeff Tucker, Dr. Agnes Janoshazi, and Erica Scappini for assistance with confocal microscopy; Dr. Chengbo Meng for assistance with the fiber photometry experiment setup; Allen Lin, Dr. Jesse Cushman, and Korey Stevanovic for the custom TTL signal generator for the fiber photometry experiments; Drs. David Armstrong, Georgia Alexander, and Jesse Cushman for helpful advice and comments on the manuscript; and the Viral Vector Core, Fluorescence Microscopy and Imaging Center, Neurobehavioral Core Laboratory, and Comparative Medicine Branch at the National Institute of Environmental Health Science for assistance with the study. This work was supported by the NIH Intramural Research Program.

1. Hasselmo ME (1999) Neuromodulation: Acetylcholine and memory consolidation. *Trends Cogn Sci* 3:351–359.
2. Buzsáki G (1996) The hippocampo-neocortical dialogue. *Cereb Cortex* 6:81–92.
3. Stickgold R (2004) Dissecting sleep-dependent learning and memory consolidation. Comment on Schabus M et al. Sleep spindles and their significance for declarative memory consolidation. Sleep 2004;27(8):1479-85. *Sleep* 27:1443–1445.
4. Rasch BH, Born J, Gais S (2006) Combined blockade of cholinergic receptors shifts the brain from stimulus encoding to memory consolidation. *J Cogn Neurosci* 18: 793–802.
5. Rasch B, Born J (2013) About sleep's role in memory. *Physiol Rev* 93:681–766.
6. Hasselmo ME, McGaughy J (2004) High acetylcholine levels set circuit dynamics for attention and encoding and low acetylcholine levels set dynamics for consolidation. *Prog Brain Res* 145:207–231.
7. Walker MP, Stickgold R (2004) Sleep-dependent learning and memory consolidation. *Neuron* 44:121–133.
8. Davies P, Maloney AJ (1976) Selective loss of central cholinergic neurons in Alzheimer's disease. *Lancet* 2:1403.
9. Whitehouse PJ, et al. (1982) Alzheimer's disease and senile dementia: Loss of neurons in the basal forebrain. *Science* 215:1237–1239.
10. Kametani H, Kawamura H (1990) Alterations in acetylcholine release in the rat hippocampus during sleep-wakefulness detected by intracerebral dialysis. *Life Sci* 47:421–426.
11. Marrosu F, et al. (1995) Microdialysis measurement of cortical and hippocampal acetylcholine release during sleep-wake cycle in freely moving cats. *Brain Res* 671:329–332.
12. Gais S, Born J (2004) Low acetylcholine during slow-wave sleep is critical for declarative memory consolidation. *Proc Natl Acad Sci USA* 101:2140–2144.
13. Kukolja J, Thiel CM, Fink GR (2009) Cholinergic stimulation enhances neural activity associated with encoding but reduces neural activity associated with retrieval in humans. *J Neurosci* 29:8119–8128.
14. Rogers JL, Kesner RP (2003) Cholinergic modulation of the hippocampus during encoding and retrieval. *Neurobiol Learn Mem* 80:332–342.

15. Nakauchi S, Brennan RJ, Boulter J, Sumikawa K (2007) Nicotine gates long-term potentiation in the hippocampal CA1 region via the activation of alpha2* nicotinic ACh receptors. *Eur J Neurosci* 25:2666–2681.
16. Fujii S, Ji Z, Morita N, Sumikawa K (1999) Acute and chronic nicotine exposure differentially facilitate the induction of LTP. *Brain Res* 846:137–143.
17. Mann EO, Greenfield SA (2003) Novel modulatory mechanisms revealed by the sustained application of nicotine in the guinea-pig hippocampus in vitro. *J Physiol* 551: 539–550.
18. Gu Z, Yakel JL (2011) Timing-dependent septal cholinergic induction of dynamic hippocampal synaptic plasticity. *Neuron* 71:155–165.
19. Burwell RD, Amaral DG (1998) Cortical afferents of the perirhinal, postrhinal, and entorhinal cortices of the rat. *J Comp Neurol* 398:179–205.
20. Insausti R, Herrero MT, Witter MP (1997) Entorhinal cortex of the rat: Cytoarchitectonic subdivisions and the origin and distribution of cortical efferents. *Hippocampus* 7: 146–183.
21. Witter MP, Van Hoesen GW, Amaral DG (1989) Topographical organization of the entorhinal projection to the dentate gyrus of the monkey. *J Neurosci* 9:216–228.
22. Remondes M, Schuman EM (2004) Role for a cortical input to hippocampal area CA1 in the consolidation of a long-term memory. *Nature* 431:699–703.
23. Canto CB, Wouterlood FG, Witter MP (2008) What does the anatomical organization of the entorhinal cortex tell us? *Neural Plast* 2008:381243.
24. Swanson LW, Köhler C (1986) Anatomical evidence for direct projections from the entorhinal area to the entire cortical mantle in the rat. *J Neurosci* 6:3010–3023.
25. Hamam BN, Kennedy TE, Alonso A, Amaral DG (2000) Morphological and electrophysiological characteristics of layer V neurons of the rat medial entorhinal cortex. *J Comp Neurol* 418:457–472.
26. Kloosterman F, Van Haeften T, Witter MP, Lopes Da Silva FH (2003) Electrophysiological characterization of interlaminar entorhinal connections: An essential link for re-entrance in the hippocampal-entorhinal system. *Eur J Neurosci* 18:3037–3052.
27. Sik A, Penttonen M, Ylinen A, Buzsáki G (1995) Hippocampal CA1 interneurons: An in vivo intracellular labeling study. *J Neurosci* 15:6651–6665.
28. Leão RN, et al. (2012) OLM interneurons differentially modulate CA3 and entorhinal inputs to hippocampal CA1 neurons. *Nat Neurosci* 15:1524–1530.
29. Maccaferri G, McBain CJ (1995) Passive propagation of LTD to stratum oriens-alveus inhibitory neurons modulates the temporoammonic input to the hippocampal CA1 region. *Neuron* 15:137–145.
30. McQuiston AR, Madison DV (1999) Muscarinic receptor activity has multiple effects on the resting membrane potentials of CA1 hippocampal interneurons. *J Neurosci* 19: 5693–5702.
31. Lawrence JJ, Statland JM, Grinspan ZM, McBain CJ (2006) Cell type-specific dependence of muscarinic signalling in mouse hippocampal stratum oriens interneurones. *J Physiol* 570:595–610.
32. Bell LA, Bell KA, McQuiston AR (2013) Synaptic muscarinic response types in hippocampal CA1 interneurons depend on different levels of presynaptic activity and different muscarinic receptor subtypes. *Neuropharmacology* 73:160–173.
33. Lawson VH, Bland BH (1993) The role of the septohippocampal pathway in the regulation of hippocampal field activity and behavior: Analysis by the intraseptal microinfusion of carbachol, atropine, and procaine. *Exp Neurol* 120:132–144.
34. Vandecasteele M, et al. (2014) Optogenetic activation of septal cholinergic neurons suppresses sharp wave ripples and enhances theta oscillations in the hippocampus. *Proc Natl Acad Sci USA* 111:13535–13540.
35. Tamamaki N, Nojyo Y (1995) Preservation of topography in the connections between the subiculum, field CA1, and the entorhinal cortex in rats. *J Comp Neurol* 353: 379–390.
36. Wickersham IR, Finke S, Conzelmann KK, Callaway EM (2007) Retrograde neuronal tracing with a deletion-mutant rabies virus. *Nat Methods* 4:47–49.
37. Wickersham IR, et al. (2007) Monosynaptic restriction of transsynaptic tracing from single, genetically targeted neurons. *Neuron* 53:639–647.
38. Sheridan RD, Sutor B (1990) Presynaptic M1 muscarinic cholinoceptors mediate inhibition of excitatory synaptic transmission in the hippocampus in vitro. *Neurosci Lett* 108:273–278.
39. Hasselmo ME, Schnell E (1994) Laminar selectivity of the cholinergic suppression of synaptic transmission in rat hippocampal region CA1: Computational modeling and brain slice physiology. *J Neurosci* 14:3898–3914.
40. Dasari S, Gulledge AT (2011) M1 and M4 receptors modulate hippocampal pyramidal neurons. *J Neurophysiol* 105:779–792.
41. Mans RA, Warmus BA, Smith CC, McMahon LL (2014) An acetylcholinesterase inhibitor, eserine, induces long-term depression at CA3-CA1 synapses in the hippocampus of adult rats. *J Neurophysiol* 112:2388–2397.
42. Siechen S, Yang S, Chiba A, Saif T (2009) Mechanical tension contributes to clustering of neurotransmitter vesicles at presynaptic terminals. *Proc Natl Acad Sci USA* 106: 12611–12616.
43. Wickelgren WO, Leonard JP, Grimes MJ, Clark RD (1985) Ultrastructural correlates of transmitter release in presynaptic areas of lamprey reticulospinal axons. *J Neurosci* 5: 1188–1201.
44. Häusser M (2014) Optogenetics: The age of light. *Nat Methods* 11:1012–1014.
45. Jackman SL, Beneduce BM, Drew IR, Regehr WG (2014) Achieving high-frequency optical control of synaptic transmission. *J Neurosci* 34:7704–7714.
46. Gähwiler BH, Brown DA, Enz A, Knöpfel T (1989) Development of the septohippocampal projection in vitro. *EXS* 57:236–250.
47. Korsching S, Auburger G, Heumann R, Scott J, Thoenen H (1985) Levels of nerve growth factor and its mRNA in the central nervous system of the rat correlate with cholinergic innervation. *EMBO J* 4:1389–1393.
48. Li Y, et al. (1995) Regulation of TrkA and ChAT expression in developing rat basal forebrain: Evidence that both exogenous and endogenous NGF regulate differentiation of cholinergic neurons. *J Neurosci* 15:2888–2905.
49. Gahwiler BH, Brown DA (1985) Functional innervation of cultured hippocampal neurones by cholinergic afferents from co-cultured septal explants. *Nature* 313: 577–579.
50. Frotscher M, Heimrich B (1995) Lamina-specific synaptic connections of hippocampal neurons in vitro. *J Neurobiol* 26:350–359.
51. Guthrie KM, Tran A, Baratta J, Yu J, Robertson RT (2005) Patterns of afferent projections to the dentate gyrus studied in organotypic co-cultures. *Brain Res Dev Brain Res* 157:162–171.
52. Osakada F, et al. (2011) New rabies virus variants for monitoring and manipulating activity and gene expression in defined neural circuits. *Neuron* 71:617–631.
53. Yizhar O, et al. (2011) Neocortical excitation/inhibition balance in information processing and social dysfunction. *Nature* 477:171–178.
54. Hooks BM, Lin JY, Guo C, Svoboda K (2015) Dual-channel circuit mapping reveals sensorimotor convergence in the primary motor cortex. *J Neurosci* 35:4418–4426.
55. Rajasethupathy P, et al. (2015) Projections from neocortex mediate top-down control of memory retrieval. *Nature* 526:653–659.
56. Zemankovics R, Káli S, Paulsen O, Freund TF, Hájos N (2010) Differences in subthreshold resonance of hippocampal pyramidal cells and interneurons: The role of h-current and passive membrane characteristics. *J Physiol* 588:2109–2132.
57. Pangalos M, et al. (2013) Recruitment of oriens-lacunosum-moleculare interneurons during hippocampal ripples. *Proc Natl Acad Sci USA* 110:4398–4403.
58. Spoida K, Masseck OA, Deneris ES, Herlitze S (2014) Gq/5-HT2c receptor signals activate a local GABAergic inhibitory feedback circuit to modulate serotonergic firing and anxiety in mice. *Proc Natl Acad Sci USA* 111:6479–6484.
59. Isoardi NA, Bertotto ME, Martijena ID, Molina VA, Carrer HF (2007) Lack of feedback inhibition on rat basolateral amygdala following stress or withdrawal from sedative-hypnotic drugs. *Eur J Neurosci* 26:1036–1044.
60. Naus CC, Morrison JH, Bloom FE (1988) Development of somatostatin-containing neurons and fibers in the rat hippocampus. *Brain Res* 468:113–121.
61. Cui G, et al. (2014) Deep brain optical measurements of cell type-specific neural activity in behaving mice. *Nat Protoc* 9:1213–1228.
62. Zhu H, et al. (2014) Chemogenetic inactivation of ventral hippocampal glutamatergic neurons disrupts consolidation of contextual fear memory. *Neuropsychopharmacology* 39:1880–1892.
63. Ishii K, Wong JK, Sumikawa K (2005) Comparison of alpha2 nicotinic acetylcholine receptor subunit mRNA expression in the central nervous system of rats and mice. *J Comp Neurol* 493:241–260.
64. Wada E, et al. (1989) Distribution of alpha 2, alpha 3, alpha 4, and beta 2 neuronal nicotinic receptor subunit mRNAs in the central nervous system: A hybridization histochemical study in the rat. *J Comp Neurol* 284:314–335.
65. Mikulovic S, Restrepo CE, Hilscher MM, Kullander K, Leão RN (2015) Novel markers for OLM interneurons in the hippocampus. *Front Cell Neurosci* 9:201.
66. Barker GR, Warburton EC (2011) When is the hippocampus involved in recognition memory? *J Neurosci* 31:10721–10731.
67. Mumby DG, Gaskin S, Glenn MJ, Schramek TE, Lehmann H (2002) Hippocampal damage and exploratory preferences in rats: Memory for objects, places, and contexts. *Learn Mem* 9:49–57.
68. Winters BD, Forwood SE, Cowell RA, Saksida LM, Bussey TJ (2004) Double dissociation between the effects of peri-postrhinal cortex and hippocampal lesions on tests of object recognition and spatial memory: Heterogeneity of function within the temporal lobe. *J Neurosci* 24:5901–5908.
69. von Linstow Roloff E, Harbaran D, Micheau J, Platt B, Riedel G (2007) Dissociation of cholinergic function in spatial and procedural learning in rats. *Neuroscience* 146:875–889.
70. Berger-Sweeney J, et al. (2001) Selective immunolesions of cholinergic neurons in mice: Effects on neuroanatomy, neurochemistry, and behavior. *J Neurosci* 21: 8164–8173.
71. Drachman DA (1977) Memory and cognitive function in man: Does the cholinergic system have a specific role? *Neurology* 27:783–790.
72. Kalisch Ellett LM, Pratt NL, Ramsay EN, Barratt JD, Roughead EE (2014) Multiple anticholinergic medication use and risk of hospital admission for confusion or dementia. *J Am Geriatr Soc* 62:1916–1922.
73. Gray SL, et al. (2015) Cumulative use of strong anticholinergics and incident dementia: A prospective cohort study. *JAMA Intern Med* 175:401–407.
74. Chrobak JJ, Buzsáki G (1994) Selective activation of deep layer (V-VI) retrohippocampal cortical neurons during hippocampal sharp waves in the behaving rat. *J Neurosci* 14:6160–6170.
75. Klausberger T, et al. (2003) Brain-state- and cell-type-specific firing of hippocampal interneurons in vivo. *Nature* 421:844–848, and erratum (2006) 441:902.
76. Varga C, Golshani P, Soltesz I (2012) Frequency-invariant temporal ordering of interneuronal discharges during hippocampal oscillations in awake mice. *Proc Natl Acad Sci USA* 109:E2726–E2734.
77. Anagnostaras SG, Gale GD, Fanselow MS (2002) The hippocampus and Pavlovian fear conditioning: Reply to Bast et al. *Hippocampus* 12:561–565.
78. Hunsaker MR, Fieldsted PM, Rosenberg JS, Kesner RP (2008) Dissociating the roles of dorsal and ventral CA1 for the temporal processing of spatial locations, visual objects, and odors. *Behav Neurosci* 122:643–650.
79. Kjelstrup KB, et al. (2008) Finite scale of spatial representation in the hippocampus. *Science* 321:140–143.
80. Buzsáki G, Moser EI (2013) Memory, navigation and theta rhythm in the hippocampal-entorhinal system. *Nat Neurosci* 16:130–138.
81. Schmid LC, et al. (2016) Dysfunction of somatostatin-positive interneurons associated with memory deficits in an Alzheimer's disease model. *Neuron* 92:114–125.